scanner consisting of an avalanche photodiode PET (APDPET) with a ToT-based application-specific integrated circuit (ASIC) and digital signal processing scheme at the front-end that utilizes leading edge timing and ToT-based energy measurement. Eight 144-channel detector modules—each having 12 × 12 Pr:LuAG–APD arrays individually coupled with ToT-based mixed signal ASICs—were constructed and configured together into a ring-shaped architecture. In Section 2, the scanner used in this fabricated PET system is explained. Details about the materials, electronics, and detectors used are provided in Section 3. A summary is given in Section 4 in which measurements and image reconstructions based on basic characteristics such as energy, time, and spatial resolution are evaluated.

2. Scanner architecture

The PET designed for this study consists of eight detector modules with 144 (12 × 12) channels each (Fig. 1). PMTID in the figure indicates the detector number in the PET system. D, Gap, Cover thickness indicate the distance (mm) between coincidence pair, the gap (mm) between two neighboring detector modules and the distance (mm) between the surface of Aluminum cover and that of Pr:LuAG crystal. In each module, one channel is composed of a Pr:LuAG crystal coupled with one APD pixel that is individually coupled with one ToT ASIC channel. Each ToT ASIC output is connected to an integrating FPGA board for multiplexing in order to reduce the number of transmission lines needed. The wired-OR multiplexing readout implemented in the FPGA reduces the number of lines from 144 to 24 (i.e., 12 lines demarking the *X* and *Y* axes, respectively) in each module (Fig. 2). The overall PET ring has 192 (24 × 8) ToT digital outputs that are processed by an ADC-based data acquisition (DAQ) system that uses a coincidence function to sum the ADC outputs for the initial evaluation. The count rate is therefore limited by the dead time (4 μs) of the DAQ system. Outputs (i.e., coincidence events) acquired by the DAQ system are sent via four Ethernet cables to a DAQ PC and a data reconstruction PC (Fig. 3). Fig. 4 shows the schematic of our DAQ. DAQ includes the summing amplifiers and the sampling ADC with 80 MHz frequency. The energy is measured by summing the ADC values for the duration of ToT, which corresponds to the pulse width of ToT signal. The dynamic range of ToT signal acceptable for the sampling ADC is up to 500 ns.

The TODPET system is designed for use as a small animal PET scanner with an aimed time resolution of ~10 ns [20].

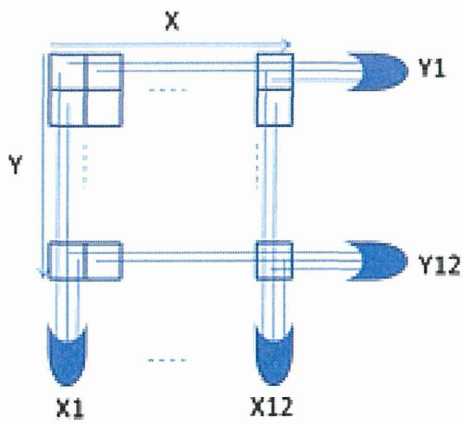

Fig. 2. *X–Y* wired-OR multiplexing readout.

3. Materials and methods

3.1. Pr:LuAG crystal arrays

Fig. 5 shows a picture of the 12 × 12 Pr:LuAG matrix developed for this system. The pixels are divided from each other by a reflective, 0.2-mm-thick $BaSO_4$ layer, and each pixel is 2 × 2 × 10 mm^3 in size.

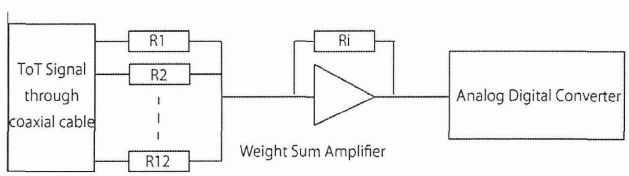

Fig. 4. DAQ system for one module.

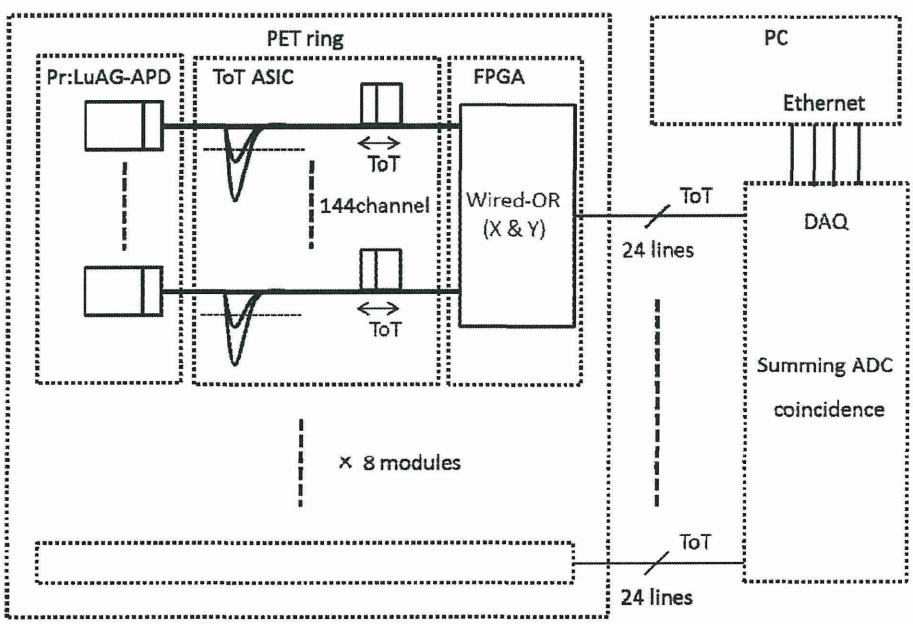

Fig. 3. Whole system of the PET system.

Owing to its interesting properties including Pr^{3+} 5d–4f emission at a wavelength of 310 nm, non-hygroscopic nature, high density (6.7 g/cm^3), high light output (around 20,000 photons/MeV), very short decay time (20 ns), and high energy resolution (4.6% at 662 keV for a $6 \times 6 \times 1$ mm^3 Pr:LuAG sample and a Hamamatsu R1791 PMT), Pr^{3}+-doped transparent ceramic $Lu_3Al_5O_{12}$ (i.e., Pr:LuAG) has attracted considerable attention [21–25]. For this study, 12×12 Pr:LuAG crystal matrix scintillators were fabricated for use as the detector modules of the APD-based PET (Fig. 1).

3.2. APDs

A 12×12 array of 144-channel Hamamatsu UV-enhanced APD detector modules coupled with LuAG scintillators at a 2-mm pixel pitch (which offers a compact platform for gamma ray detection) was fabricated as shown in Fig. 6. The array has an area of 31.8 mm^2 and a quantum efficiency of 55% at 310 nm when coupled with the LuAG scintillators [26]. At a gain of 50, the APD produces a dark current on the order of 0.1–0.7 nA, and the bias voltage must be set to 380 V to achieve a gain of ~100. Variation of the gain among the pixels is within 15% for a gain of 50. Each of the 144 Pr:LuAG crystals in the array is individually coupled with an APD.

3.3. Readout electronics

The readout electronics for the scanner system consist of three custom-designed ToT-based ASICs, and all outputs from the ASIC are connected to a Cyclone II FPGA in order to enable flexible digital signal processing and multiplexing. The readout chip utilizes 48 ToT channels, each consisting of a charge sensitive preamplifier and a leading edge-type discriminator to produce both timing and energy information over a binary readout channel. Fig. 7 shows a picture of a custom ASIC used for TODPET. The ASIC was fabricated using 0.25-μm 3.3-V Taiwan Semiconductor Manufacturing Company complementary metal-oxide-semiconductor (TSMC CMOS) technology and has a power consumption of 230 mW per chip and a die size of 5×2 mm^2.

The individual threshold of each chip is controlled by 12-bit off-chip threshold-controlling digital-to-analog converters (DACs). Six DACs, an AC coupling resistor-capacitor (RC) network, and the ToT-based ASICs are mounted on a 3×6 cm^2 front-end printed circuit board (Fig. 8). In the figure, the left-hand side of the board is connected to the APD detector, and the right-hand side is connected to an FPGA board. The pitch of the threshold adjustment applied by the DACs equals 0.8 mV.

A charge sensitive preamplifier with a designed gain of 5 V/pC and a measured noise level of ~1200 electrons at full width at half-maximum (FWHM) is used. The effect of the measured

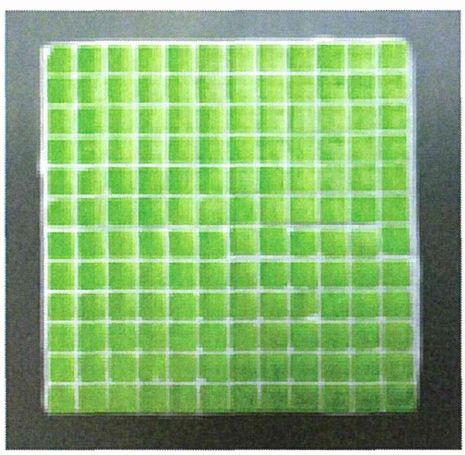

Fig. 5. 12×12 Pr:LuAG crystal array used in APDPET.

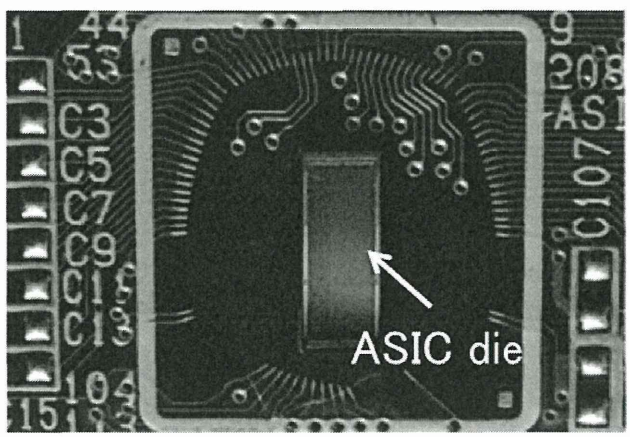

Fig. 7. Custom-designed ToT ASIC (5×2 mm^2).

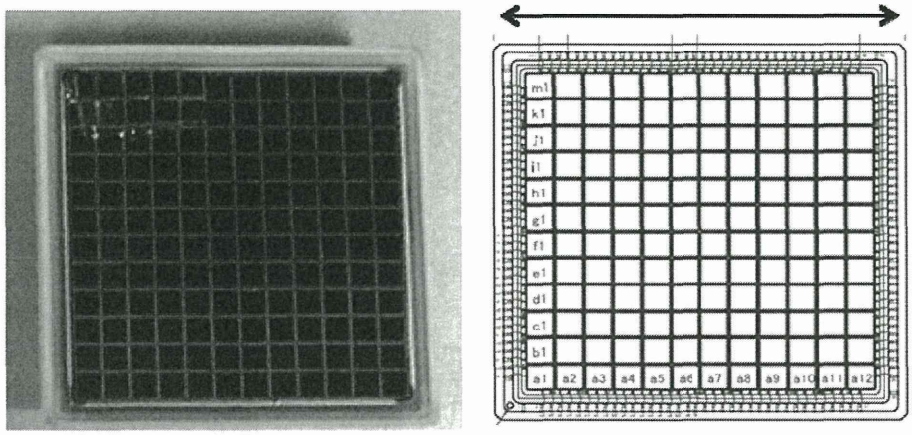

Fig. 6. 12×12 array composing the 144-channel UV-enhanced APD detector.

electric noise is low enough (0.95% at an energy of 20 fC) for the application to function correctly. Fig. 9 shows a comparison between the measured relationship between the ToT and input charge. Here, the typical measured duration of the ToT digital output is between 100 and 300 ns over a range of 10–60 fC, which matches well with the calculated results. Fig. 10 shows the threshold variation between the 48 ASIC channels; this is within

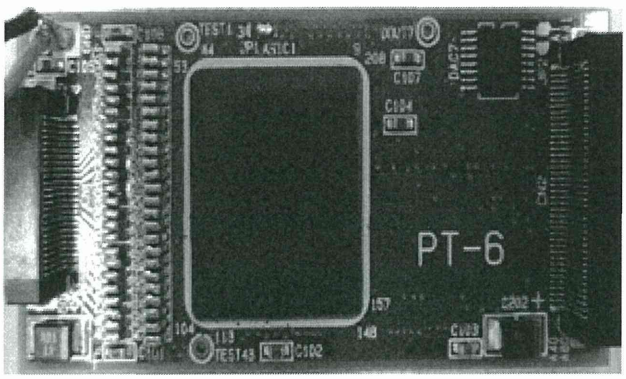

Fig. 8. Front-end ASIC board for TOT-based APDPET.

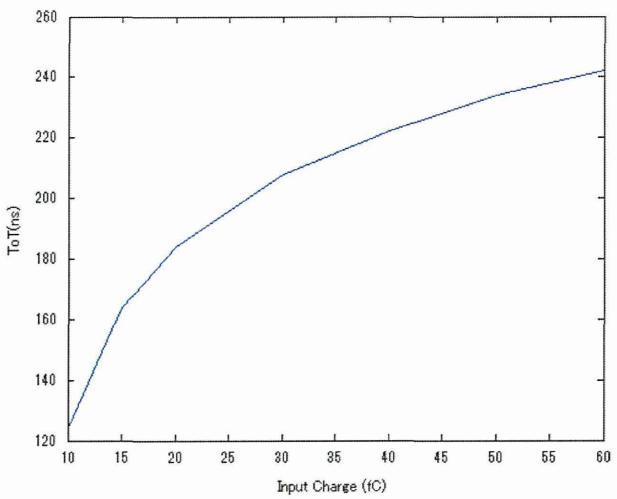

Fig. 9. Measured relation between input charge and time for the ToT-based ASIC.

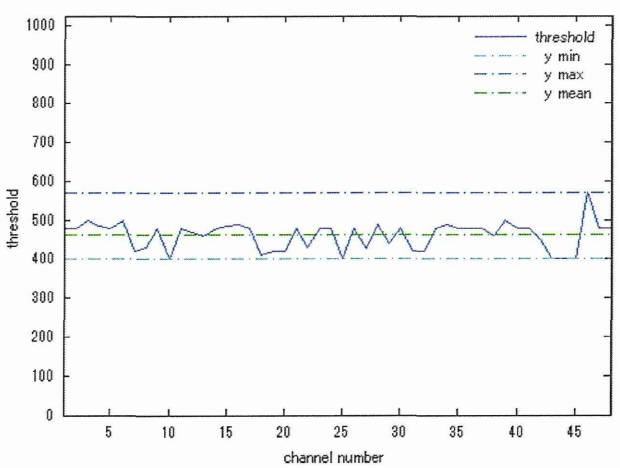

Fig. 10. Threshold variation in the front-end chip (unit for the vertical axis is DAC code, which corresponds to about 0.8 mV).

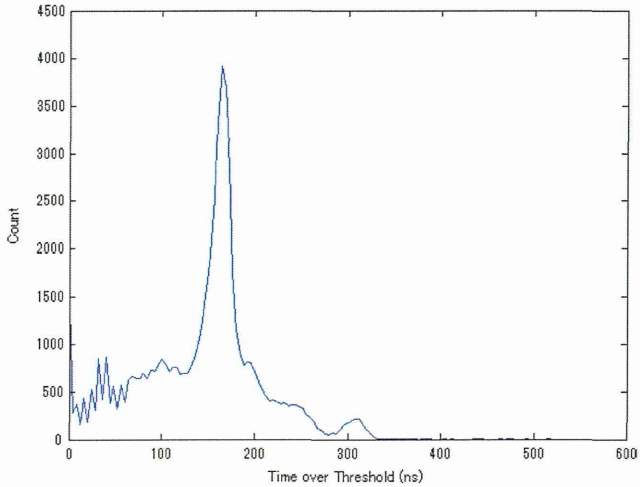

Fig. 11. Energy spectrum of 511-keV gamma rays from a ^{22}Na source measured with the ToT output by an Altera Cyclone III FPGA.

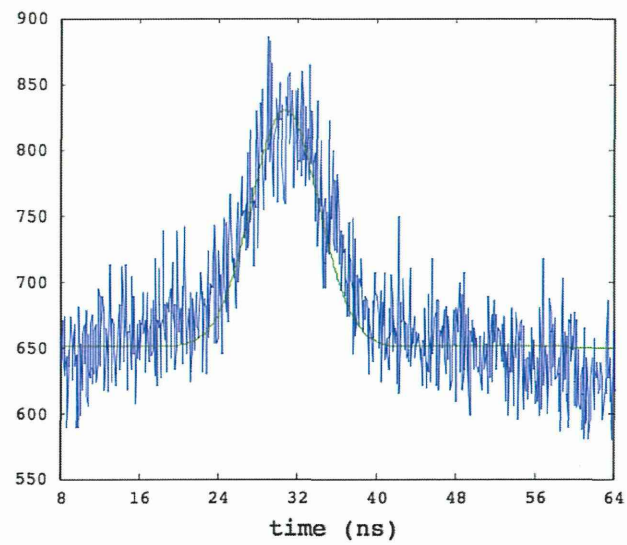

Fig. 12. Time resolution for 511-keV annihilation gamma rays measured with two coincidence modules.

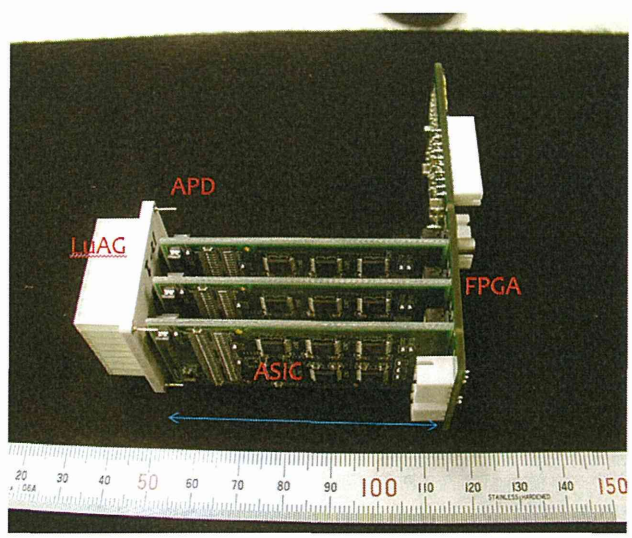

Fig. 13. TODPET detector module.

160 mV and was adjusted using the external 12-bit DACs in the experiment. As threshold adjustment for each channel is necessary in order to obtain proper ToT output, it is applied to all channels.

3.4. Detector module

Fig. 11 shows the digital ToT measurements for the energy spectrum of a typical channel for 511-keV gamma rays from a ^{22}Na source. The ToT pulse duration is measured using a Cyclone-III-based FPGA with a 250-MHz clock, the sampling frequency of which caused a degradation of energy resolution of 5% at a time width of 160 ns. The figure shows clear peaks for 511 keV and a 1.28-MeV photopeak; the corresponding non-calibrated energy resolution of ~10% (FWHM) at 511 keV indicates that this module functions well as a PET detector [27].

Using two opposing detector modules, the coincidence time resolution is measured for 511-keV annihilation gamma rays from a ^{22}Na source by means of a HRMTime time-correlated single photon counting (TCSPC) module (SensL Co.). Without the application of an energy window, the time resolution for coincidence is measured to be 6.0 ns FWHM, and the time resolution for one detector module is calculated as 4.2 ns. This result is well within the operating specifications of the ~20 ns timing window specified for the animal system in this study, and the threshold of each channel can be optimized using 12-bit off-chip DACs controlled by an FPGA board (Fig. 12).

All 144 channels of the Pr:LuAG–APD detector are individually connected to the ToT ASIC channels. A charge sensitive preamplifier in the ToT ASIC converts a charge signal to a voltage signal; this is then converted by a ToT circuit with a discriminator into a digital

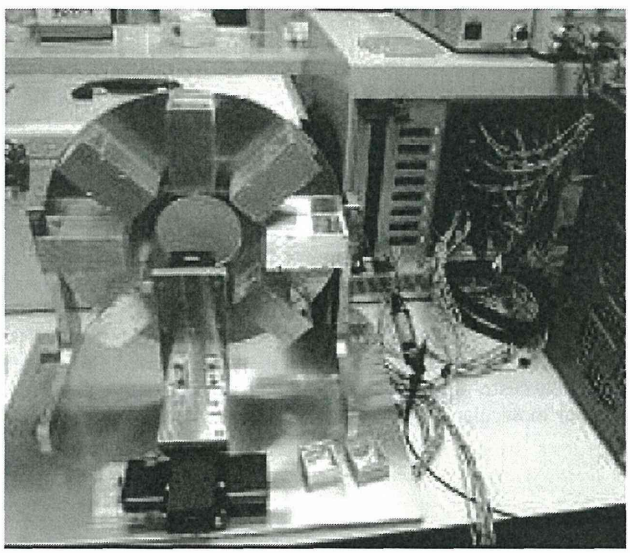

Fig.14. PET system with eight detector modules.

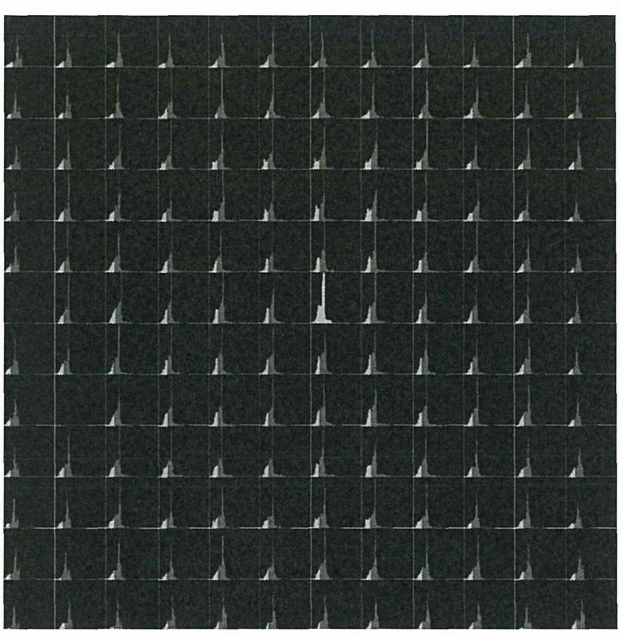

Fig. 15. Measured energy spectra of 144 channels in one detector module.

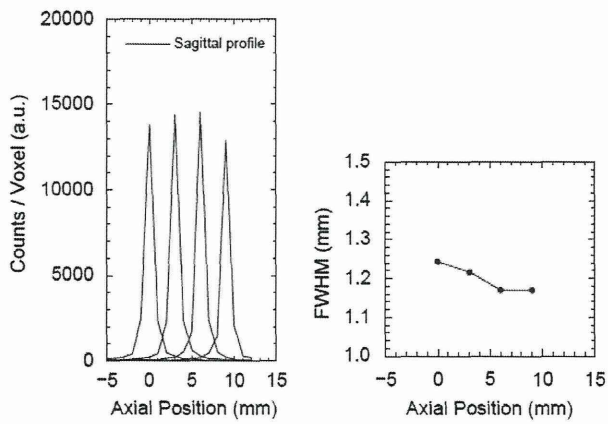

Fig. 16. Simulated resolution with Monte-Carlo simulation (sagittal profile depending on the axial position).

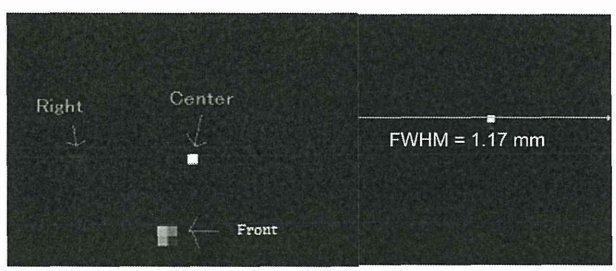

Fig. 17. Measured three point sources of ^{22}Na (center, right, and front)).

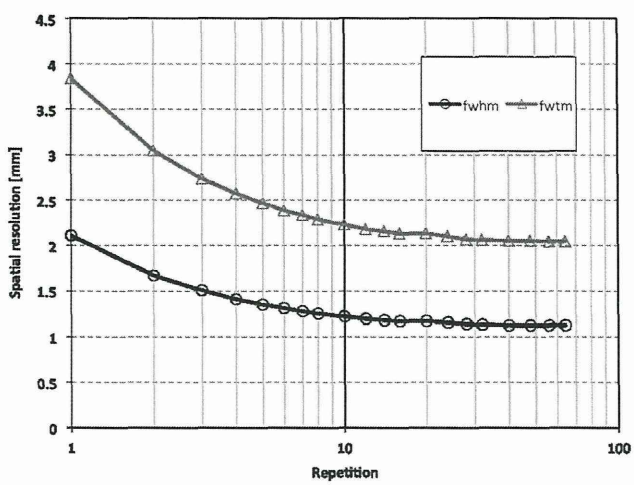

Fig. 18. Spatial resolution versus iteration.

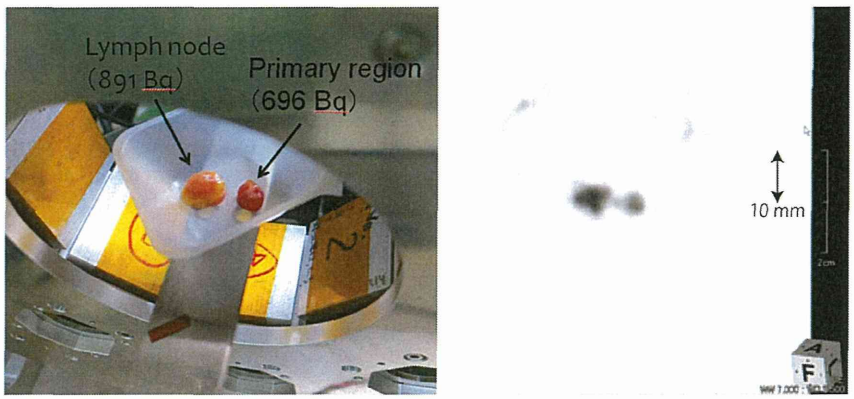

Fig. 19. Samples of gastric cancers and a reconstructed image.

pulse of specified duration. All ToT outputs are connected to an Altera Cyclone II FPGA, which integrates and multiplexes these for transmission to the DAQ system. The FPGA board also communicates with the threshold controlling DACs.

Fig. 13 shows the assembled readout module consisting of the 144-channel PET detector (composed of a 12×12 pixel LuAG crystal and a 12×12 pixel APD), three 48-channel front-end ASIC boards, and one FPGA digital processing circuit inserted into the motherboard. The length of the detector is about 9 cm including the detector and its electronics.

4. Results

4.1. Image reconstruction

A complete PET detector ring system consisting of eight detector modules spaced at 72.5 mm (crystal-to-crystal) was built (Fig. 14); the detector modules were covered and fixed in place using a solid aluminum frame. The resulting position map is completely separated, with 95% of the detector pixels successfully working (the malfunctioning of 5% of the pixels is caused by damage to the front-end ASIC or APD pixels). The energy spectra of the channels are shown in Fig. 15.

Using GEANT4, a point source image with a field of view (FOV) diameter of 34.5 mm and an axial depth of 25 mm was simulated by means of a maximum-likelihood expectation maximization (MLEM) reconstruction algorithm. Simulations revealed axial and radial spatial resolutions of $\sim$1.2 mm and $\sim$2.5 mm, respectively Fig. 16.

An image is acquired and successfully reconstructed with 1 MBq ^{22}Na point sources; Fig. 17 shows the images representing the point sources at three different positions reconstructed after 20 MLEM iterations at a pixel size of 1×1 mm^2. The pixel size of the reconstructed image is set as the half-size of the crystal. The measured spatial resolutions are 1.17 mm at FWHM (center) in the first preliminary reconstruction result. Fig. 18 shows the spatial resolution depending on the number of iterations.

An image is also acquired with the samples of a gastric cancer and a surrounding lymph node which has the strength of 696 Bq and 891 Bq (Fig. 19). The measurement was carried out for 20 min. The two samples are clearly described in the reconstructed image. A pool phantom was for the normalization of images with the condition using ^{18}FDG (250 μCi, 12 h). The measured sensitivity (CPS) is 842 ± 51 cps per 1 MBq ^{18}FDG in the measurements.

5. Conclusion

For this study, a PET scanner based on the ToT method is developed. In order to achieve high spatial resolution, the PET is composed of 144-channel Pr:LuAG–APD detectors individually coupled with custom-designed ToT ASICs. This design provides a simple front-end circuit able to use flexible digital signal processing and multiplexing techniques such as the pulse train method. The measured energy resolution of the PET system is 10% at the 511-keV peak, and a 4.25-ns time resolution is measured using a single detector module. The initial measured spatial resolution from a point source (a columnar ^{22}Na source) is 1.17 mm at FWHM. These results lead us to believe that this ToT-based PET system with fully customizable ASICs has the potential to serve as a useful tool for molecular imaging with high flexibility.

References

[1] S.R. Cherry, Y. Shao, R.W. Silverman, K. Meadors, S. Siegel, A. Chatziioannou, J.W. Young, W. Jones, J.C. Moyers, D. Newport, A. Boutefnouchet, T.H. Farquhar, M. Andreaco, M.J. Paulus, D.M. Binkley, R. Nutt, M.E. Phelps, IEEE Transactions on Nuclear Science NS-44 (3) (1997) 1161.
[2] A.P. Jeavons, R.A. Chandler, C.A.R. Dettmar, IEEE Transactions on Nuclear Science NS-46 (3) (1999) 468.
[3] P. Vaska, C.L. Woody, D.J. Schlyer, S. Shokouhi, S.P. Stoll, J.-F. Pratte, P. O'Connor, S.S. Junnarkar, S. Rescia, B. Yu, M. Purschke, A. Kandasamy, A. Villanueva, A. Kriplani, V. Radeka, N. Volkow, R. Lecomte, R. Fontaine, IEEE Transactions on Nuclear Science NS-51 (5) (2004) 2718.
[4] M. Streun, G. Brandenburg, H. Larue, C. Parl, K. Ziemons, IEEE Transactions on Nuclear Science NS-53 (3) (2006) 700.
[5] S. Surti, J.S. Karp, A.E. Perkins, C.A. Cardi, M.E. Daube-Witherspoon, A. Kuhn, G. Muehllehner, IEEE Transactions on Medical Imaging 24 (7) (2005) 844.
[6] C.-M. Kao, Q. Xie, Y. Dong, L. Wan, C.-T. Chen, IEEE Transactions on Nuclear Science NS-56 (5) (2009) 2678.
[7] H. Alva-Sanchez, T. Murrieta, E. Moreno-Barbosa, M.E. Brandan, C. Ruiz-Trejo, A. Martinez-Davalos, M. Rodriguez-Villafuerte, IEEE Transactions on Nuclear Science NS-57 (1) (2010) 85.
[8] S. Yamamoto, M. Honda, T. Oohashi, K. Shimizu, M. Senda, IEEE Transactions on Nuclear Science NS-58 (3) (2011) 668.
[9] M. Bergeron, J. Cadorette, J.-F. Beaudoin, M.D. Lepage, G. Robert, V. Selivanov, M.-A. Tetrault, N. Viscogliosi, J.P. Norenberg, R. Fontaine, R. Lecomte, IEEE Transactions on Nuclear Science NS-56 (1) (2009) 10.
[10] J. Kataoka, H. Matsuda, F. Nishikido, M. Koizumi, H. Ikeda, M. Yoshino, T. Miura, S. Tanaka, Y. Ishikawa, N. Kawabata, K. Shimizu, Y. Matsunaga, S. Kishimoto, H. Kubo, Y. Yanagida, T. Nakamori, IEEE Transactions on Nuclear Science NS-57 (5) (2010) 2448.
[11] D.P. McElroy, W. Pimpl, B.J. Pichler, M. Rafecas, T. Schuler, S.I. Ziegler, IEEE Transactions on Nuclear Science NS-52 (1) (2005) 199.
[12] R. Lecomte, Nuclear Instruments and Methods in Physics Research A 527 (1-2) (2004) 157.
[13] V.Ch. Spanoudaki, D.P. McElroy, S.I. Ziegler, Nuclear Instruments and Methods in Physics Research Section A: Accelerators, Spectrometers, Detectors and Associated Equipment 564 (1) (2006) 451.

[14] M. Rafecas, I. Torres, V. Spanoudaki, D.P. McElroy, S.I. Ziegler, Nuclear Instruments and Methods in Physics Research Section A: Accelerators, Spectrometers, Detectors and Associated Equipment 571 (1–2) (2007) 285.
[15] F. Powolny, E. Auffray, H. Hillemanns, P. Jarron, P. Lecoq, T.C. Meyer, D. Moraes, IEEE Transactions on Nuclear Science NS-55 (5) (2008) 2465.
[16] P.D.,Olcott; C.S., Levin, Pulse width modulation: a novel readout scheme for high energy photon detection, in: Proceedings of the Nuclear Science Symposium Conference Record (NSS '08), October 19–25, 2008, pp. 4530–4535.
[17] K. Shimazoe, H. Takahashi, B. Shi, T. Furumiya, J. Ooi, Y. Kumazawa, H. Murayama, IEEE Transactions on Nuclear Science NS-57 (2) (2010) 782.
[18] Z. Deng, A.K. Lan, X. Sun, C. Bircher, Y. Liu, Y. Shao, IEEE Transactions on Nuclear Science NS-58 (6) (2011) 3212.
[19] C. Parl, H. Larue, M. Streun, K. Ziemons, S. Van Waasen, IEEE Transactions on Nuclear Science NS-59 (5) (2012) 1809.
[20] Daniel Strul Luc Simon, Giovanni Santin, Magalie Krieguer, Christian Morel, Nuclear Instruments and Methods in Physics Research Section A: Accelerators, Spectrometers, Detectors and Associated Equipment 527 (1–2) (2004) 190.
[21] T., Yanagida; M., Sato; K., Kamada; A., Yoshikawa; F., Saito, Evaluation of gamma-ray responses of LuAG(Pr) scintillator coupled with APD, in: Proceedings of the Nuclear Science Symposium Conference Record (NSS '07), vol. 2, October 26–November 3, 2007, pp. 1338–1342.
[22] K. Kamada, T. Yanagida, K. Tsutsumi, Y. Usuki, M. Sato, H. Ogino, A. Novoselov, A. Yoshikawa, M. Kobayashi, S. Sugimoto, F. Saito, IEEE Transactions on Nuclear Science NS-56 (3) (2009) 570.
[23] Kei Kamada Takayuki Yanagida, Noriaki Kawaguchi, Yutaka Fujimoto, Kentaro Fukuda, Yuui Yokota, Valery Chani, Akira Yoshikawa, Nuclear Instruments and Methods in Physics Research Section A: Accelerators, Spectrometers, Detectors and Associated Equipment 652 (1) (2011) 256.
[24] Takayuki Yanagida Kei Kamada, Yoshiyuki Usuki, Akira Yoshikawa, Nuclear Instruments and Methods in Physics Research Section A: Accelerators, Spectrometers, Detectors and Associated Equipment 610 (1) (2009) 215.
[25] K. Kamada, T. Yanagida, T. Endo, K. Tsutumi, M. Yoshino, J. Kataoka, U. Usuki, Y. Fujimoto, A. Fukabori, A. Yoshikawa, Journal of Crystal Growth 352 (1) (2012) 91.
[26] M. Yoshino, J. Kataoka, T. Nakamori, H. Matsuda, T. Miura, T. Katou, Y. Ishikawa, N. Kawabata, Y. Matsunaga, K. Kamada, Y. Usuki, A. Yoshikawa, T. Yanagida, Nuclear Instruments and Methods in Physics Research A 643 (1) (2011) 57.
[27] Kenji Shimazoe, Tadashi Orita, Yasuaki Nakamura, Hiroyuki Takahashi, Time over threshold based multi-channel LuAG-APD PET detector, Nuclear Instruments and Methods in Physics Research Section A: Accelerators, Spectrometers, Detectors and Associated Equipment, Volume 731, 11 December 2013, Pages 109–113.

Development of a Prototype Detector Using APD-Arrays Coupled With Pixelized Ce:GAGG Scintillator for High Resolution Radiation Imaging

Kei Kamada, Kenji Shimazoe, Shigeki Ito, Masao Yoshino, Takanori Endo, Kousuke Tsutsumi, Jun Kataoka, Shunsuke Kurosawa, Yuui Yokota, Hiroyuki Takahashi, and Akira Yoshikawa

Abstract—**A novel digital PET scanner based on Time over Threshold method is developed. The positron emission tomography (PET) is composed of 144channel Ce:$Gd_3Al_2Ga_3O_{12}$ (GAGG)-Avaranche photodiode (APD) detector arrays individually coupled with custom designed Time over Threshold (ToT) application-specific integrated circuit (ASIC) to realize the high count rate and good spatial resolution. Such an imaging system provides a simple front-end circuit and flexible digital signal processing like multiplexing such as a pulse train method. The measured energy resolution of the detector system was 6.7% for the 511 keV peak, and 4.25 ns time resolution was measured with a single detector module. The measured spatial resolution for a point source was 1.37 mm FWHM for our initial data with a columnar ^{22}Na source.**

Index Terms—**Avalanche photodiode (APD), positron emission tomography (PET), scintillator.**

I. Introduction

SCINTILLTORS coupled with Si based photodiode have been widely used in many applications, such as high energy physics, astrophysics, and medical imaging. Recently, demands for a gamma camera detecting gamma-rays from ^{131}I, ^{134}Cs, ^{137}Cs, etc., have been increasing after the accidents in the Fukushima Daiichi nuclear power plant. In these applications, scintillators require such properties as good energy resolution, high stopping power, high light yield, and fast decay. In addition, positron emission tomography (PET) is a very effective tool to analyze the distribution of target molecules and plays an important role in small-animal molecular imaging. The precise imaging of radio-labeled tracers is necessary for biological research to reveal the function of a biological system. Therefore, many PET scanners have been designed and developed for animal PET systems and the theoretical limit of spatial resolution may be within reference [1]–[12]. Also, some PET scanners are developed using the individual readout method to achieve both high count rate capability and better spatial resolution. However, the individual readout system introduces complex and power-consuming front-end signal processing hardware, such as analog-to-digital converters (ADCs) for the energy measurement and time-to-digital converters (TDC) for the timing measurement [13]. Recently, digital signal processing using a Field Programmable Gate Array (FPGA) has become a very powerful technology.

Thus, matching between the emission wavelength of scintillators and sensitive wavelengths of Avaranche photodiode (APD) is also very important. Recently, Ce:$Gd_3Al_2Ga_3O_{12}$ (Ce:GAGG) has attracted attention because of its interesting properties, such as Ce^{3+} 5d-4f emission peaking at 520 nm, high density (6.63 g/cm^3), high light output (around 48,000 photon/MeV), fast decay time (88 ns), very low level of natural radioactivity, and good energy resolution of 4.8%@662 keV [14]–[18]. In this paper, we demonstrate the performance of a prototype detector using a 12×12 channel APD-array coupling with Ce:GAGG array. Three 48-channel front-end application-specific integrated circuit (ASIC) boards are inserted into the APD-array and motherboard with the FPGA digital processing circuit. The assembled detector modules with 144-channel gamma-ray detector were developed. Performance of the detector and position mapping results using coincidence mode were examined.

II. Detectors and Electronics

A. Scintillatior Arrays and APD-arrays

A 50 mm diameter boule of Ce1%:GAGG was grown by the Czochralski (Cz) method and 2 × 2 × 5 mm^3 size sample

Manuscript received May 24, 2013; revised July 26, 2013; accepted September 05, 2013. Date of publication January 24, 2014; date of current version February 06, 2014. This work was supported in part by (i) the funding program for next generation world-leading researchers, JSPS, (ii) Development of Systems and Technology for Advanced Measurement and Analysis, Japan Science and Technology Agency (JST), (iii) Adaptable and Seamless Technology Transfer Program through Target-driven R&D (A-STEP), JST, (iv) Japan Society for the Promotion of Science (JSPS) Grant-in-Aid for Exploratory Research (A.Y), (v) JSPS Research Fellowships for Young Scientists (S. Kurosawa), and (vi) the Health Labour Sciences Research Grant, The Ministry of Health Labour and Welfare.

K. Kamada and Y. Yokota are with the New Industry Creation Hatchery Center (NICHe), Tohoku University, Sendai, Miyagi 980-8579, Japan (e-mail: kamada@imr.tohoku.ac.jp).

K. Kamada is with C&A Corporation, Sendai, Miyagi 980-8579, Japan.

K. Shimazoe and H. Takahashi are with the Department of Bioengineering, University of Tokyo, Tokyo 113-8656, Japan.

S. Ito, M. Yoshino, T. Endo, and K. Tsutsumii are with the Materials Research Laboratory, Furukawa Co. Ltd, Tsukuba 305-0856, Japan.

J. Kataoka is with the Research Institute for Science and Engineering, Waseda University, Shinjuku, Tokyo, Japan.

S. Kurosawa is with the Institute for Material Research, Tohoku University, Sendai 980-8577, Japan.

A. Yoshikawa is with the New Industry Creation Hatchery Center (NICHe), Tohoku University, Sendai, Miyagi 980-8579, Japan, and also with C&A Corporation, Sendai, Miyagi 980-8579, Japan, and with the Institute for Material Research, Tohoku University, Sendai 980-8577, Japan.

Color versions of one or more of the figures in this paper are available online at http://ieeexplore.ieee.org.

Digital Object Identifier 10.1109/TNS.2013.2290319

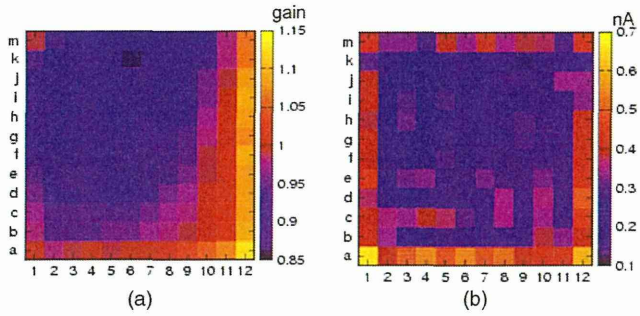

Fig. 1. (a) Gain uniformity and (b) dark current distributions of the APDarray, operated at a gain of 100.

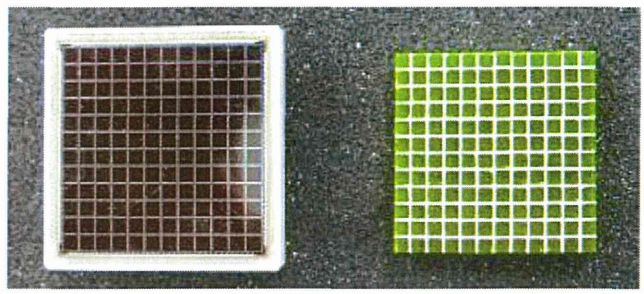

Fig. 2. Pictures of a 12 × 12 APD array (left) and 12 × 12 Ce:GAGG matrix (right).

pieces were cut and polished in Furukawa Co. Ltd. The sample showed 50,000 photon/MeV and energy resolution of 5.6% at 662 keV by the $2 \times 2 \times 5$ mm^3 size sample using a APD S8664-55 (Hamamatsu). The APD-array described here was designed with the technology of S8664 APD series (reverse-type). The APD-array has a 12×12 pixel structure with an active area of 2.05×2.05 mm^2 per pixel and a 0.25 mm gap between the pixels. The APD-array allows stable operation at a gain around 100, with extremely low dark noise (less than 1.81 nA/pixel) for each pixel, even at room temperature ($+18°$C). An avalanche gain of 100 is achieved with bias voltage of 388 V. Gain uniformity and dark current distribution of the APD-array operated at a gain of 100 are shown in Fig. 1. Note the excellent uniformity of avalanche gain (left) with low leakage current distributions (right). Gain fluctuation was characterized by direct irradiation on each APD pixels using ^{55}Fe x-ray source and the gain fluctuation is only $\pm 8\%$ over the APD device.

Finally, a prototype gamma-ray camera consisting of the APD-array optically coupled with a Ce:GAGG matrix was fabricated. Fig. 2 shows pictures of the 12×12 Ce:GAGG matrix and APD array, where each pixel is $2 \times 2 \times 5$ mm^3 in size and divided with a reflective $BaSO_4$ layer of 0.25 mm thickness. The performance of the Ce:GAGG matrix was tested by taking the energy spectrum of a ^{137}Cs source. The APD signals were fed into a preamplifier (Clear Pulse 581 K) and a shaping amplifier (ORTEC 570; shaping time 2 μs), and finally digitized with a multichannel analyzer (Amptek MCA8000A). We operated the APD-arrays under bias voltages of 330 V. All the data were taken at $+18°$C. Fig. 3 shows an example of an energy spectrum obtained with a single pixel in the APD-Ce:GAGG matrix for the ^{137}Cs source. The energy resolution of the 662 keV gamma-rays is 5.9% (FWHM). The variation of energy resolution and signal amplitude (due to inhomogeneities of APD gain and Ce:GAGG light yield) was only $\pm 1.6\%$ and 33%, respectively (Fig. 3).

B. Readout Electronics

Readout electronics consist of three custom-designed Time over Threshold (ToT) based ASICs, and all outputs from the ASIC are connected to a Cyclone II FPGA, which enables flexible digital signal processing and multiplexing. The analog and digital circuits are integrated in this chip and a window-type multi-level threshold discriminator was implemented using a digital encoder. The ToT pulse is generated when the signal is between the lower level discriminator (LLD) and upper level discriminator (ULD). The digital circuit generates two pulses with widths after the first ToT trigger pulse (see Fig. 5). The readout chip includes 48-channel ToT function to produce both the timing information and the energy information in a binary readout channel, and each channel consists of a charge-sensitive preamplifier and a leading-edge-type discriminator. The individual threshold of the chip is controlled by 12-bit off-chip threshold-controlling DACs [19]. The DACs, an AC coupling RC network, and the ASICs are mounted on a 3×6 cm^2 front-end board (see Fig. 6). The range of the threshold adjustment equals 0.8 mV. The gain of a charge-sensitive preamplifier is designed to be 5 V/pC and the measured noise level was ~1,200 electrons FWHM. The noise level was satisfactory for both timing and energy resolutions. The typical duration of ToT digital output is from 100 to 400 ns, which matches with the simulation results. The threshold variation in the designed ASIC was within 160 mV and can be adjusted with 12-bit DACs.

C. Detector Module

Fig. 7 shows the energy resolution for 511 keV gamma-rays from a Na^{22} source measured using ToT digital output. The pulse duration of ToT is measured using a Cyclone III based FPGA with a 250 MHz clock. It shows clear 511 keV and 1.28 MeV photo-peaks, and an energy resolution of 6.7% (FWHM) @ 511 keV that is good enough for gamma-camera, SPECT and PET detector.

Fig. 8 shows a readout system for our gamma-ray detector system. All 144 channels of a GAGG-APD detector are individually connected to the channels of a ToT ASIC. In the ToT ASIC, a charge-sensitive preamplifier converts a charge signal to a voltage signal, and the ToT circuit with a discriminator converts it into a digital pulse with some duration. All the ToT outputs are connected to an Altera Cyclone II FPGA. The FPGA integrates the ToT outputs and multiplexes them to send to the Data Acquisition System (DAQ). The FPGA board also communicates with the threshold-controlling DACs.

Fig. 9 shows the coincidence time resolution for 511 keV annihilation gamma rays from ^{22}Na source using two opposing detector modules. The measured time resolution is 6 ns FWHM for coincidence without energy window. The time resolution for one detector module is calculated to be 4.2 ns. Time resolution is measured with a HRMTime TCSPC module (from SensL Co.). This result is well within the operating specification of our

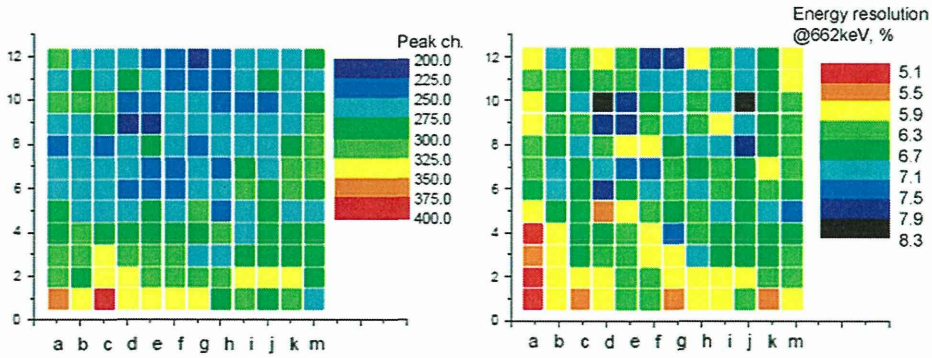

Fig. 3. The variation of energy resolution and signal amplitude in the APD-Ce:GAGG matrix for the ^{137}Cs source.

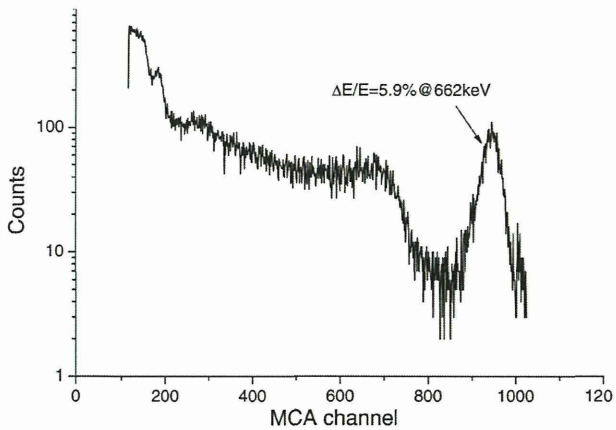

Fig. 4. Example of an energy spectrum obtained with a single pixel in the APD-Ce:GAGG matrix for the ^{137}Cs source.

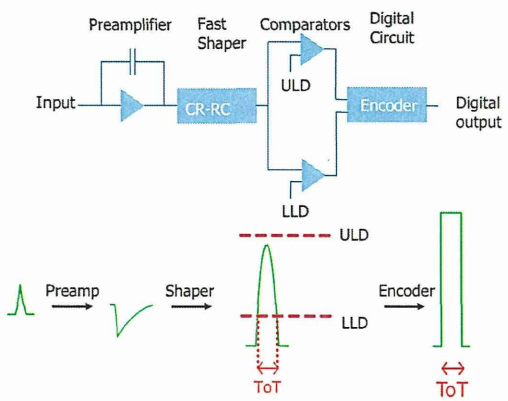

Fig. 5. Schematic drawing of ToT based signal processing method.

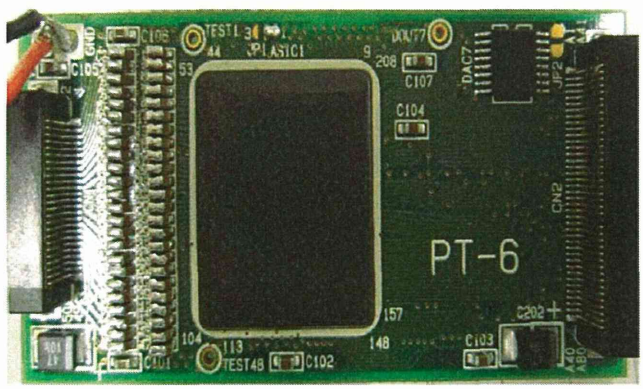

Fig. 6. Front-end ASIC board for the gamma detector.

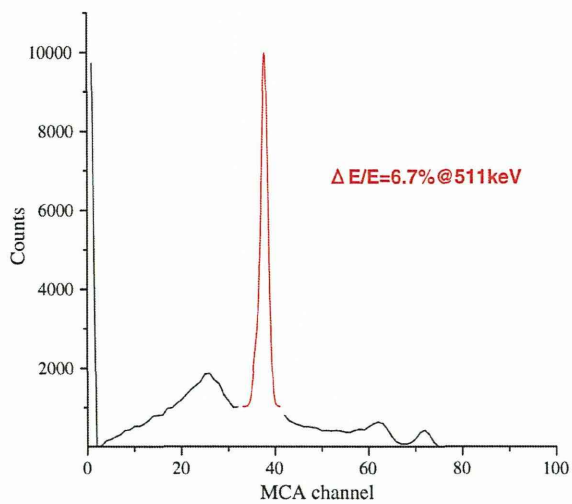

Fig. 7. Energy resolution for 511 keV gamma rays from Na^{22} source measured with ToT output by Altera Cyclone III FPGA.

animal system ~ 20 ns timing window. The threshold of each channel can be optimized with 12-bit off-chip DACs controlled by an FPGA board.

D. Image Reconstruction

The dual-headed PET system is built with two gamma-ray detector modules to form a detector ring (Fig. 10) and the detector modules are covered and fixed with an aluminum-based solid frame. A simple X and Y wired OR logic is used to reduce the number of transmission lines from 144 to 24, which are then read out by a DAQ. Five percent of the pixels are not working because of damage to the channel of the front-end ASIC or APD pixels. The energy spectra of all the channels are shown in Fig. 11.

The detector ring size is designed to be 72.5 mm (crystal to crystal). The FOV has a diameter of 25 mm by axial direction of 25 mm. We have measured a point source of ^{22}Na and successfully reconstructed an image with ML-EM reconstruction

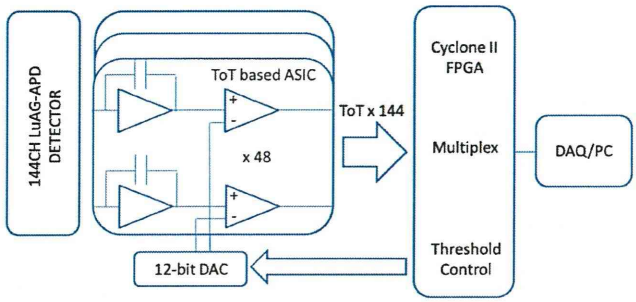

Fig. 8. Overall layout of the readout system for the imaging system module. The 144-channel LuAG-APD detector is individually connected to the ToT based ASIC. The FPGA handles and multiplexes the digitized data and controls off-chip 12-bit DACs.

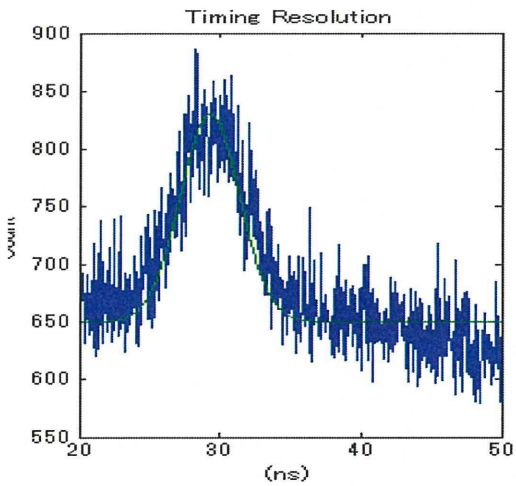

Fig. 9. Time resolution for 511 keV annihilation gamma-rays measured with two coincidence modules.

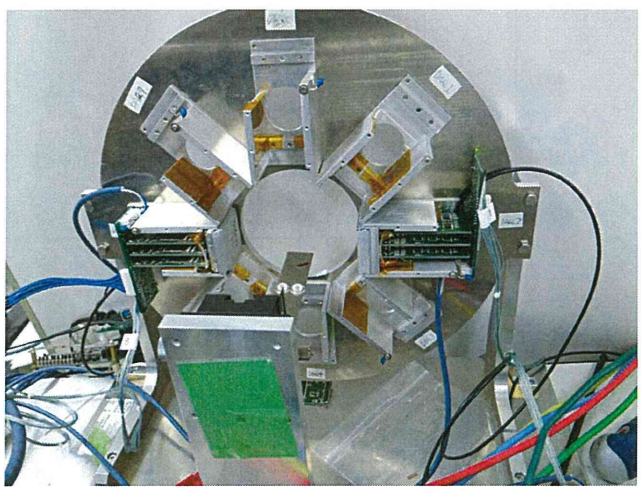

Fig. 10. The PET system with two detector modules.

algorithm. Fig. 12 shows the image of the reconstructed point source. The measured spatial resolution is 1.37 mm FWHM.

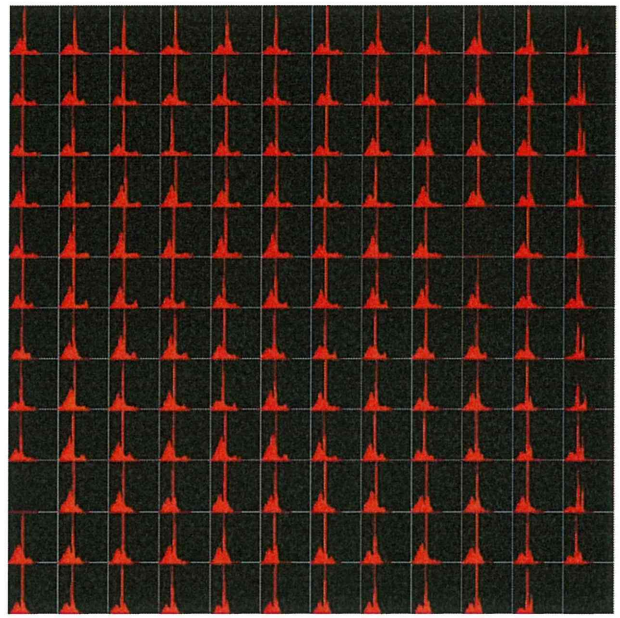

Fig. 11. Measured energy spectra of 144 channels in one detector module.

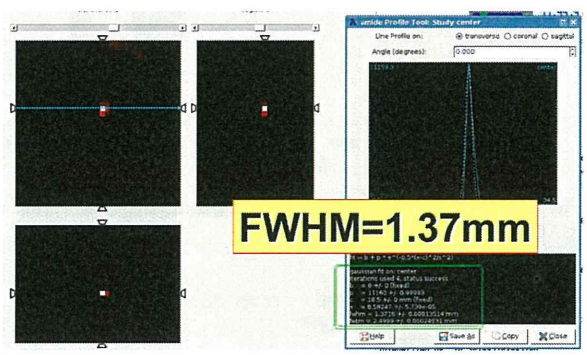

Fig. 12. Reconstructed image of a point source of ^{22}Na.

III. Conclusion

A novel digital PET scanner based on the Time over Threshold (ToT) method has been developed. The PET is composed of 144-channel GAGG-APD detector arrays and individually coupled custom-designed ToT ASICs to realize high count rate and good spatial resolution. Such an imaging system provides a simple front-end circuit and flexible digital signal processing like multiplexing such as a pulse train method. The measured energy resolution of the detector system was 6.7% for the 511 keV peak, and 4.25 ns time resolution was measured with a single detector module. The measured spatial resolution for a point source was 1.37 mm FWHM for our initial data with a columnar ^{22}Na source. We think our imaging system with fully custom ASICs will be a useful tools for molecular imaging with high flexibility. These results suggest that the detector using APD and Ce:GAGG arrays are promising devices not only for PET but also SPECT and gamma-camera applications. In addition, demands for ^{137}Cs hot-spot imaging using a gamma-camera has increased in Japan after the accidents in the Fukushima Daiichi nuclear power